Applied Catalysis B: Environmental 130–131 (2013) 36–43

Contents lists available at SciVerse ScienceDirect

Applied Catalysis B: Environmental

journal homepage: www.elsevier.com/locate/apcatb

Catalytic abatement of trichloroethylene over Mo and/or W-based bronzes

N. Blanch-Raga, M.D. Soriano, A.E. Palomares, P. Concepción, J. Martínez-Triguero*, J.M. López Nieto

Instituto de Tecnología Química, UPV-CSIC, Campus de la Universitat Politècnica de València, Avda. Los Naranjos s/n, 46022, Valencia, Spain

ARTICLE INFO

Article history:
Received 25 July 2012
Received in revised form 12 October 2012
Accepted 15 October 2012
Available online 26 October 2012

Keywords:
Catalytic oxidation
Chlorinated VOCs
Trichloroethylene
Mo–W–O mixed oxides bronzes

ABSTRACT

In this paper we present the results of the synthesis, characterization and catalytic behaviour of Mo(W)–Nb–V–O mixed metal oxides bronzes for the catalytic oxidation of trichloroethylene. The catalysts were prepared hydrothermally with different Mo/W/Nb/V/P atomic ratio and heat-treated at 500 and 700 °C. They were characterized by several techniques as N_2-adsorption, X-ray diffraction, FTIR, SEM-EDS, temperature programmed desorption, temperature programmed reduction, UV–vis, Fourier transformed infrared spectroscopy of adsorbed pyridine and $^{18}O/^{16}O$ isotope exchange. X-ray diffraction patterns (XRD) of samples heat-treated at 500 °C suggest the presence of a semi-crystalline material with a diffraction peak at ca. $2\theta = 22.2°$, while XRD patterns of samples heat-treated at 700 °C show the formation of a tetragonal tungsten bronze (TTB) structure. The activity for the catalytic abatement of trichloroethylene strongly depends on the heat-treatment temperature and the catalyst composition. Thus, samples with W/(Mo + W) atomic ratios of 0.25-0.75 and heat-treated at 500 °C are the most active ones. The enhanced activity has been related to the remarkable higher surface area of the catalyst and to the catalyst composition which influences the acid characteristics as well as the reducibility and reoxidation of the catalysts. The importance of the oxygen dissociation on the catalyst surface and the diffusion of oxygen species through the catalyst are also discussed.

1. Introduction

Volatile organic compounds (VOCs) have been regarded as an important source of environmental pollution. Particularly, chlorinated VOCs require a special attention on account of their toxicity, high stability and widespread application in industry. Their emissions result in problems related to the ozone layer destruction, photochemical smog and groundwater pollution. One of the most common chlorinated VOC is trichloroethylene (TCE), a pollutant that has been classified as probably carcinogenic to humans by the International Agency for Research on Cancer (IARC) [1].

Thus, removal of chlorinated volatile organic compounds becomes an important issue. Thermal incineration is the most commonly used process to reduce the emissions of VOCs from stationary sources. However, it requires a high temperature (>700 °C) generating important energetic costs and it also leads to the formation of non desired chlorinated by-products. Another option is the catalytic oxidation. It is considered as an effective method for the removal of hazardous compounds, such as chlorinated hydrocarbons, at low temperature (250–550 °C) [2–7].

Usually, two types of catalysts have been studied for the chlorinated VOCs abatement: metal oxides [8–20], either single (e.g. chromium oxide) or mixed (e.g. perovskites) and supported noble metals [21–26]. For both types of catalysts, deactivation is one of the main problems [7]. In this way, noble metals are very active, however, they can be easily poisoned by chlorine. On the other hand, chromium oxides are active [27], but their application is restricted to low operation temperatures because the formation of volatile and very toxic chromium oxychloride can occur. In the last years, new catalysts based in zeolites have been proposed as active catalysts for this reaction obtaining interesting results [28–32]. Nevertheless it is still necessary to find more active and stable materials.

Mo and/or W-containing tetragonal tungsten bronzes (TTB) are active and stable catalytic systems for the partial oxidation of olefins [33,34] and for the partial oxidation of H_2S to sulphur [35]. Moreover, the catalytic performance of these materials depends on the heat-treatment temperature and/or on the presence of metal oxide promoters.

In the present work we report the catalytic behaviour for the oxidation of trichloroethylene of Mo and/or W-containing mixed metal oxides, heat-treated at 500 or 700 °C, and presenting an amorphous or a tetragonal tungsten bronze (TTB) structure, respectively. The catalysts have been characterized by several techniques, in order to correlate their catalytic activity with their

* Corresponding author. Tel.: +34 96 387 78 11.
E-mail address: jomarti@itq.upv.es (J. Martínez-Triguero).

0926-3373/$ – see front matter © 2012 Elsevier B.V. All rights reserved.
http://dx.doi.org/10.1016/j.apcatb.2012.10.016

physico-chemical characteristics, in terms of catalyst composition and reducibility–reoxidation properties.

2. Experimental

2.1. Catalysts preparation

Mo-and/or W-containing catalysts presenting a tetragonal tungsten bronze (TTB) structure have been prepared by hydrothermal synthesis (at 175 °C for 48 h) from solutions containing $H_3PMo_{12}O_{40}$ or $H_3PW_{12}O_{40}$ (Aldrich), vanadyl sulphate (Aldrich), and niobium(V) oxalate (CBMM, Brazil), in order to achieve synthesis gels with a Mo/W/Nb/V/P atomic ratio of $1/1-x/0.17/0.20/0.08$ (x = 0–1) [33]. The solid obtained was filtered off, washed, dried at 80 °C for 16 h, and finally heat-treated at 500 or 700 °C for 2 h in flowing N_2. Materials were named as MWx-Y, where x is the W/(Mo + W) atomic ratio and Y corresponds to the heat-treatment temperature of 500 °C (MWx-L series) or 700 °C (MWx-H series).

An acid zeolite was used as a catalytic reference. It was prepared from a MOR zeolite (CBV-10AH, Zeolyst Intl.) in its ammonium form, with a SiO_2/Al_2O_3 molar ratio of 14. The zeolite was transformed into the H-form by calcination in air at 500 °C for 3 h, with a surface area of 490 $m^2\,g^{-1}$.

2.2. Catalysts characterization

The catalysts surface areas were measured on a Micromeritics ASAP 2000 instrument by adsorption of nitrogen.

Powder X-ray diffraction patterns (XRD) were collected using an Enraf Nonius FR590 sealed tube diffractometer, with a monochromatic Cu $K_{\alpha 1}$ source operating at 40 kV and 30 mA.

Scanning electron microscopy (SEM) micrographs were collected in a JEOL 6300 microscope operating at 20 kV, 2×10^{-9} A, beam current and 15 mm as working distance. The quantitative EDS analysis was performed using an Oxford LINK ISIS System with the SEMQUANT programme, which introduces the ZAF correction. The counting time was 100 s for major and minor elements.

Infrared spectra were recorded at room temperature in the 300-4000 cm^{-1} region with a Nicolet 205×B spectrophotometer equipped with a data station at a spectral resolution of 4 cm^{-1} and accumulations of 128 scans. Dried samples (20 mg) were mixed with 100 mg of dry KBr and pressed into a disc (600 kg cm^{-2}).

Diffuse-Reflectance (DR) UV–vis spectra were collected on a Cary 5 equipped with a 'Praying Mantis' attachment from Harrick [36].

Temperature programmed reduction (TPR) experiments were carried out on 10-20 mg of catalyst with a N_2:H_2 flow (10% H_2) of 50 ml min^{-1}. The heating rate from room temperature to 800 °C was 10 °C min^{-1}.

Temperature programmed desorption of ammonia (TPD) experiments were carried out on a TPD/2900 apparatus from Micromeritics, where 300 mg of sample was pre-treated in a He stream at 450 °C for 1 h. Ammonia was chemisorbed by pulses at 100 °C until equilibrium was reached. Then, the sample was fluxed with an He stream for 15 min, prior to increase the temperature up to 500 °C in a helium stream of 100 ml min^{-1} and using a heating rate of 10 °C min^{-1}. The NH_3 desorption was monitored by both thermal conductivity detector (TCD) and mass-spectrometer, following the characteristic mass of ammonia at m/e = 15.

Acidity of samples was also measured by infrared spectra of adsorbed pyridine in a Nicolet 710 FTIR spectrophotometer. Wafers of 10 mg cm^{-2} were mounted in a pyrex vacuum cell fitted with CaF_2 windows. Samples were pre-treated overnight at 400 °C and then cooled at room temperature to obtain the original IR spectra. Then, pyridine was admitted at room temperature, degassed at 150 °C for 1 h in order to remove the physisorbed fraction, and the spectra was registered at room temperature.

Temperature programmed isotopic exchange experiments (TPIE) were performed using a quartz microreactor coupled to a quadrupole mass spectrometer (Omnistar, Balzers) used for on-line monitoring of the exit gas composition. The temperature was raised from 25 °C to 650 °C at a heating rate of 10 °C min^{-1}. In all cases, the catalyst (0.160 g) was exposed to a 2% $^{18}O_2$/Ar flow (22 ml min^{-1}). Before the oxygen-isotopic exchange experiments the catalysts were pre-treated: (i) in O_2/Ar mixture (2% $^{16}O_2$/Ar, flow of 36 ml min^{-1}) at 450 °C for 2.5 h; (ii) cooling down to 150 °C in the same O_2/Ar mixture; (iii) once achieved 150 °C, oxygen was replaced by Argon (20 ml min^{-1}) and kept for 1.5 h at that temperature; (iv) cooling down to 25 °C. The concentration profiles were obtained by acquiring the mass spectra signals relative to $^{16}O_2$ (m/e = 32), $^{16}O^{18}O$ (m/e = 34) and $^{18}O_2$ (m/e = 36). Blank run experiments were performed using an empty reactor in order to check contributions of the gas-phase reactions, and the stability of the mass spectrometer.

2.3. Catalysts activity

Catalytic oxidation reactions were carried out in a conventional quartz fixed bed reactor under atmospheric pressure. The catalyst bed (0.68 g) was supported on a quartz plug located into the reactor. Silicon monocarbide (>0.42 mm o.d.) was placed above the catalyst bed as a preheating zone of the incoming feed stream. The temperature was measured with a K-thermocouple located inside the reactor, right before the catalyst bed. The reactor was housed in an electrically-heated furnace.

The flow rate through the reactor was set at 400 ml min^{-1} and the gas hourly space velocity (GHSV) was maintained at 15,000 h^{-1}. The residence time, based on the packing volume of the catalyst, was 0.24 s. The chlorinated compound was injected into the dry air with a syringe pump in order to obtain a TCE concentration of 1000 ppm and the reaction temperature was varied from 100 to 550 °C in steps of 50 °C. Each temperature was kept during 30 min, being the overall length of the reaction 6 h.

Gases were analyzed using a Varian 3900 gas chromatograph (GC) equipped with a flame ionization detector (FID) and a HP-5 column. CO and CO_2 were separated using a Brucker 450 gas chromatograph equipped with a thermal conductivity detector (TCD) and micro-packed columns.

Analysis of both Cl_2 and HCl was performed by bubbling the effluent stream through a water solution. The concentration of chloride ions in the bubbled solution was determined by using an ion selective electrode.

3. Results and discussion

3.1. Catalyst characterization

Fig. 1 shows the XRD patterns of samples heat-treated at 500 °C (Fig. 1A) and at 700 °C (Fig. 1B). Semi-crystalline material, with an intense diffraction peak at ca. 2θ = 22.2° (i.e. ca. 4 Å), is mainly observed in the W-free sample heat treated at 500 °C (Fig. 1A, pattern a). This diffraction peak shifts to higher values when increasing the W/(Mo + W) ratio, and it is observed at ca. 2θ = 22.8° in the Mo-free sample (Fig. 1A, pattern e). On the other hand the XRD patterns of the samples heat-treated at 700 °C show the appearance of a crystalline phase. Thus, the diffraction patterns of the W-free sample, heat-treated at 700 °C, show the main peaks at 2θ = 22.2°, 23.1°, 26.6°, 30.5°, 33.2° and 35.0°, which can be assigned to the unit cell of the tetragonal tungsten bronzes (TTB) structure (JCPDS

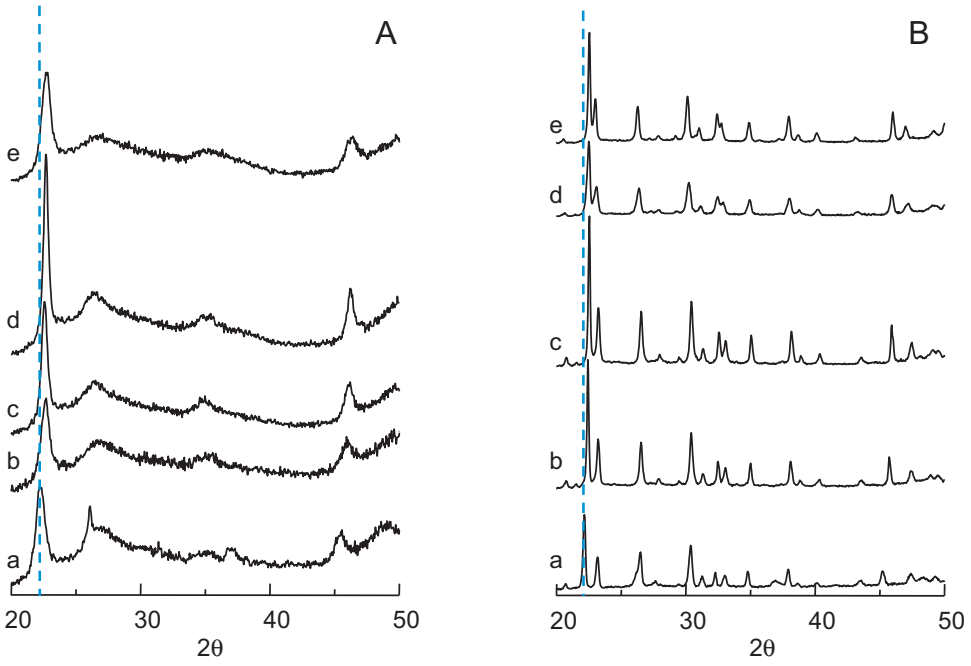

Fig. 1. XRD patterns of samples heat-treated at 500 °C (A) or 700 °C (B): (a) MW0; (b) MW25; (c) MW50; (d) MW75; (e) MW100.

file No. 80-02136) [34] (Fig. 1B, pattern a). Other minor phases are not detected in these materials. Similar patterns have been also observed in the samples where Mo is replaced by W, although some of the diffraction peaks shift to different values. In this way, peaks at $2\theta = 22.6°$, 23.0°, 26.3°, 30.2°, 32.8° and 34.9° are observed in the Mo-free sample (Fig. 1B, pattern e). The shift to higher 2θ of the first main peak in XRD patterns in samples heat-treated at 500 °C and 700 °C can be related to unit cell changes as a consequence of the replacement of Mo by W in the framework [37].

Table 1 shows a summary of the most important physical and chemical characteristics of these materials. As it can be seen, solids heat-treated at 700 °C present a lower surface area than those heat-treated at 500 °C, as a consequence of their higher crystal size. This is in agreement with previous results obtained over Te-promoted catalysts with similar structure [38,39].

X-ray energy dispersive spectroscopy (X-EDS) microanalysis shows a homogenous distribution of both elements (Mo and W) in every analyzed spot. On the other hand, although chemical composition of heat-treated materials matches reasonably well with synthesis gel composition, some differences were observed (Table 1). Thus, molybdenum is generally incorporated to a larger extent than tungsten during the hydrothermal synthesis. In addition, V and Nb contents slightly increase when increasing the W/Mo ratio. These results suggest that a higher concentration of tungsten atoms could facilitate a higher incorporation of vanadium or niobium in the framework of the TBB structure.

Fig. 2 presents the infrared spectra of samples heat-treated at 500 °C (Fig. 2A) and at 700 °C (Fig. 2B). The spectra of the samples heat-treated at 700 °C show bands at 940, 879-859, 748, 630-640, 538 and 445 cm^{-1}, associated to Me = O stretching vibration and to (Mo, W)–O–Y (Y = Mo, W, V, Nb) bridges vibrations (879-859, 748, 630-640, 538 and 445 cm^{-1}) [38,39], No important changes are observed in samples heat-treated at 500 °C (Fig. 2A). In fact, broad bands at 904, 757, 618-620 and 537-522 cm^{-1} are mainly

Table 1
Characteristics of heat-treated catalysts.

Sample	W/(Mo + W) mol ratio in gel	Catalyst composition[a]	S_{BET}[b]	TPR results	TPD[d]	
		Mo/W/Nb/V/P		H_2-uptake[c]	$\mu mol_{NH_3}\ g^{-1}$	$\mu mol_{NH_3}\ m^{-2}$
MW0-L	0	1.00/0.00/0.48/0.16/0.11	73.2	8.02	319	4.4
MW25-L	0.25	0.70/0.30/0.41/0.20/0.08	84.6	3.86	253	3.0
MW50-L	0.50	0.54/0.46/0.41/0.20/0.08	81.5	1.41	331	4.1
MW75-L	0.75	0.48/0.52/0.55/0.23/0.16	89.0	0.91	243	2.7
MW100-L	1.0	0.00/1.00/0.86/0.29/0.06	95.3	0.41	218	2.3
MW0-H	0	1.00/0.00/0.48/0.16/0.11	3.0	4.98		
MW25-H	0.25	0.70/0.30/0.41/0.20/0.08	n.d	n.d		
MW50-H	0.50	0.54/0.46/0.41/0.20/0.08	12.3	1.86		
MW75-H	0.75	0.48/0.52/0.55/0.23/0.16	n.d	n.d		
MW100-H	1.0	0.00/1.00/0.86/0.29/0.06	14.4	0.30		

[a] Atomic composition of heat-treated samples determined by EDS.
[b] Surface area in $m^2\ g^{-1}$ of the catalysts.
[c] H_2-uptake (in $mmol_{H_2}\ g^{-1}$) achieved during the TPR experiments.
[d] NH_3-TPD results: amount of NH_3 adsorbed in $\mu mol_{NH_3}\ g^{-1}$ or $\mu mol_{NH_3}\ m^{-2}$ of the catalysts heat-treated at 500 °C.

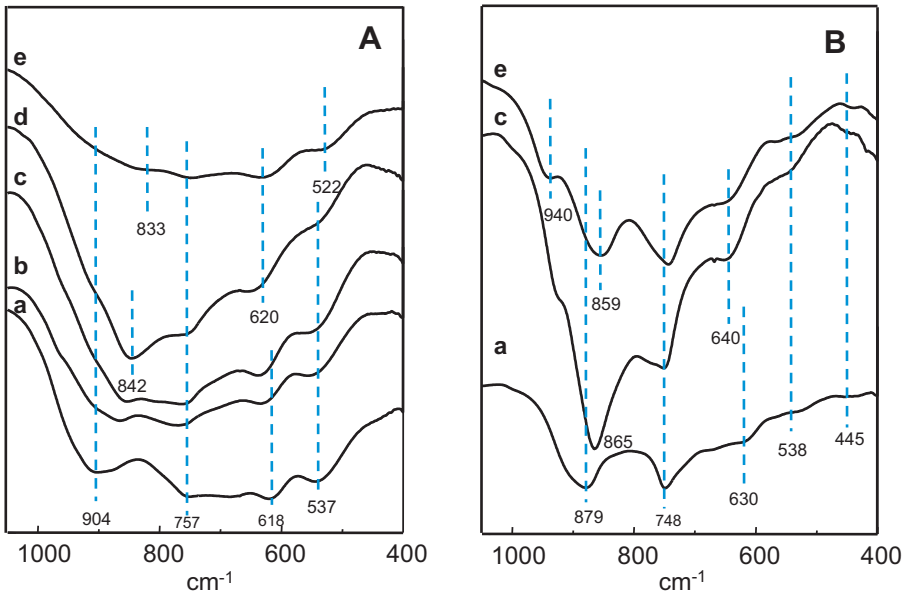

Fig. 2. FTIR spectra of samples heat-treated at 500 °C (A) or 700 °C (B): (a) MW0; (b) MW25; (c) MW50; (d) MW75; (e) MW100.

observed. The broadness of the bands is probably a consequence of the higher heterogeneity of these samples, in agreement to their less crystalline structure as determined by XRD.

Fig. 3 shows the Diffuse Reflectance UV–vis spectra of samples heat-treated at 500 °C. Two different regions corresponding to the ultraviolet (UV), from 200 to 450 nm, and to the visible (VIS), from 500 to 700 nm, can be analyzed. In the visible region, the W-free sample spectra (MW-0) show bands at 574 nm and 650 nm (Fig. 3, spectra a and b), which suggest the presence of Mo and V in oxidation states lower than 6+ and 5+, respectively. The band at 650 nm is also observed in the case of Mo-free sample (Fig. 3, spectrum c), indicating that V(4+) species are also present in this catalyst [40].

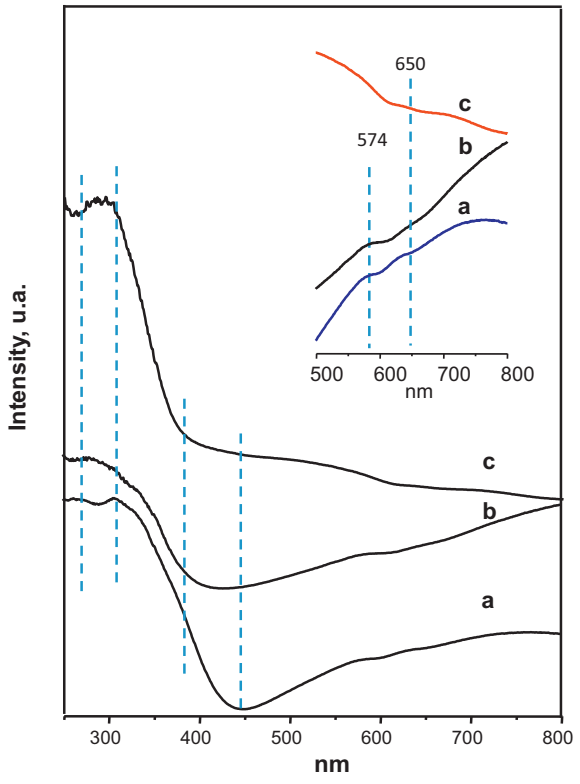

Fig. 3. Diffuse reflectance UV–vis spectra of the catalysts heat-treated at 500 °C: (a) MW0-L; (b) MW50-L; (c) MW100-L.

However, the assignment of bands in the 200–450 nm range is difficult because the signals of many species converge, i.e. Mo^{6+} (250-400 nm) [40,41], V^{5+} (250-450 nm) [42], and Nb^{5+} (235-310 nm) [43]. Moreover, the band at ca. 290 nm in Mo-free catalyst can be related to the presence of octahedral W(6+) species as in polytungstates [44,45] and in W-based bronzes [46], while the absence of a band at 400 nm confirms the absence of WO_3 crystals [47].

H_2-TPR is frequently used to study the redox property of metal oxide catalysts. Fig. 4 presents the H_2-TPR profiles on bronze catalysts. It can be seen that the measured area of the first reduction signal decreases when vanadium and molybdenum species are replaced by W species, suggesting that V and Mo are involved in the reduction of these materials in the temperature range of 300-600 °C (L-series) and 400-650 °C (H-series). Thus, the first peak can be assigned to the reduction of Mo and V species and the second one can be assigned to the partial decomposition of the catalyst structure and the reduction of W. However, the amount of each reduced specie cannot be easily quantified because their oxidation state changes when the W-content of the samples is increased. On the other hand, comparing the samples heat-treated at 500 °C (Fig. 4A) with the samples heat-treated at 700 °C (Fig. 4B), it can be observed that the maximum of H_2-uptake appears at ca. 100 °C lower in the samples heat-treated at 500 °C than in the samples heat-treated at 700 °C, indicating that samples heat-treated at 500 °C are more easy to reduce.

NH_3-TPD profiles of the samples, MW0-L, MW50-L and MW100-L, were determined by mass spectrometry (m/e = 15) and are shown in Fig. 5A (and Table 1). All samples show a first desorption peak at approximately 200-220 °C and a second desorption peak in the 250-300 °C temperature range. However, the importance of the second peak increases when increasing the W-content, suggesting that W-containing samples present acid sites with higher acid strength. For this reason and in order to clarify the characteristics of the acid sites, the same three samples have been also studied

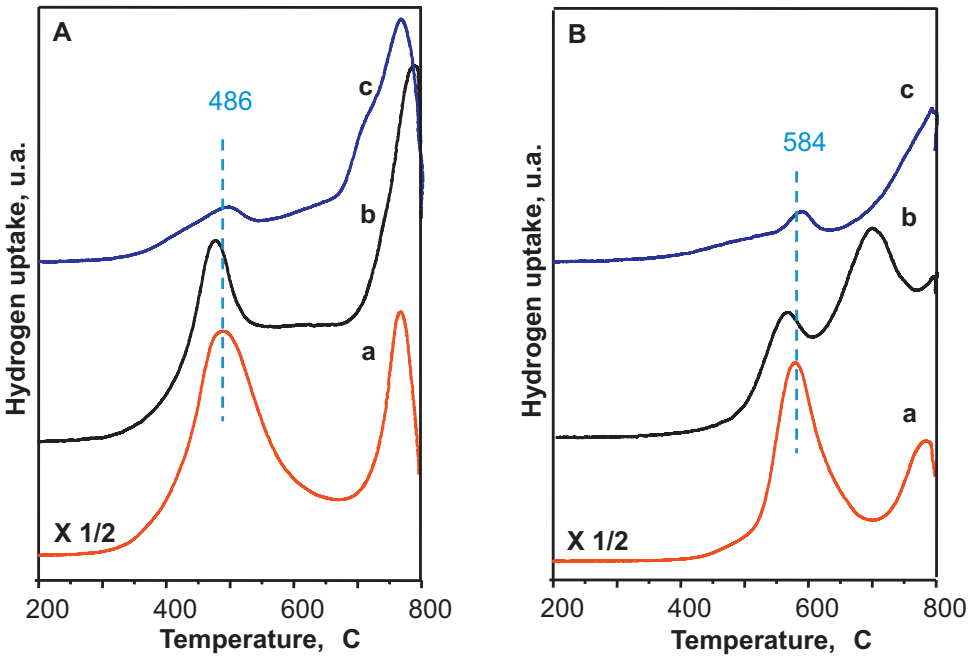

Fig. 4. H_2-TPR patterns of the catalysts heat-treated at 500 °C (A) or 700 °C (B): (a) MW0; (b) MW50; (c) MW100.

by FTIR of adsorbed pyridine, in the 1350-1750 cm^{-1} region, after desorption at 150 °C (Fig. 5B). Bands at 1446, 1490 and 1610 cm^{-1} are associated to pyridine coordinated to Lewis acid sites, while bands at 1535 and 1638 cm^{-1} are related to pyridinium cations in Brönsted acid sites [48] (Fig. 5B). When comparing the results achieved on these samples, it can be concluded that Brönsted acid sites are only present in W-containing samples, while the number of Lewis acid sites decreases according to the following trend: MW100-L > MW50-L > MW0-L.

Temperature programmed $^{18}O_2$ isotopic exchange measurements (TPIE) have been performed on samples heat-treated at 500 °C, in order to study the nature of the oxygen species participating in the combustion reaction [49].

The oxygen exchange process begins at lower temperature on the W-free sample (370 °C) compared to the higher temperature observed on the Mo,W-containing samples (480 °C on MW25-L and MW50-L) or on the Mo-free sample (530 °C) (Fig. 6). This behaviour indicates changes in the mobility of oxygen species in these catalysts depending on the catalyst composition. In addition, a different distribution of isotopic oxygen species is observed on these samples depending on the W/(Mo+W) ratio. Thus, the amount of double exchanged $^{16}O^{18}O$ (which involves diatomic oxygen exchange between $^{18}O_2$ and adjacent pairs of $^{16}O^{2-}$ or between $^{18}O_2$ and peroxy-type $(^{16}O^{-}–^{16}O^{-})_{(s)}$ on the surface of the catalyst) decreases when increasing the W-content in catalyst (Fig. 6, left). However, the amount of exchanged $^{16}O_2$ (i.e. at the bulk level) is

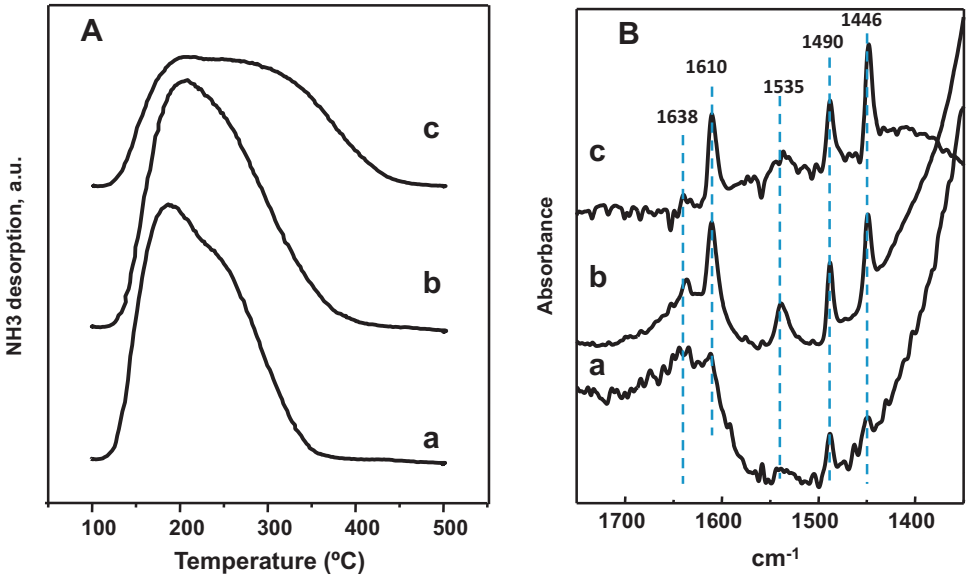

Fig. 5. NH_3-TPD patterns (A) and I.R. spectra of adsorbed pyridine at a desorption temperature of 150 °C (B) of catalysts heat-treated at 500 °C: (a) MW0-L; (b) MW50-L; (c) MW100-L.

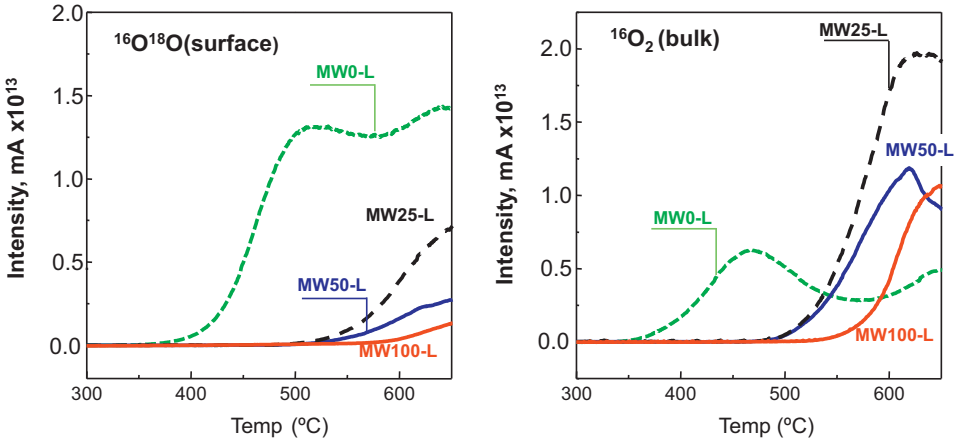

Fig. 6. Evolution of the oxygen exchange ($^{16}O^{18}O$ and $^{16}O_2$) formation species versus temperature during TPIE experiments of samples heat-treated at 500 °C.

higher in the catalysts containing both Mo and W that in the W-free sample (Fig. 6, right).

In this way, the W-free sample (i.e. MW0-L), shows a higher amount of double exchanged $^{16}O^{18}O$ than that of exchanged $^{16}O_2$, suggesting that the oxygen dissociation in the catalyst surface is faster than its diffusion into the bulk, enhancing the concentration of active electrophilic species on the catalyst surface. However, W-containing samples show a higher amount of $^{16}O_2$, indicating that the diffusion of oxygen species into the bulk is faster than the oxygen dissociation. Thus, it can be concluded that the incorporation of tungsten in the catalyst increases the diffusion of oxygen in the bulk which, under catalytic conditions, could facilitate a fast reoxidation of the catalyst. Accordingly, the catalysts preferred in a combustion reaction should be those presenting relatively high amount of cross-labelled $^{16}O^{18}O$ species but with the higher amount of doubly exchanged $^{16}O_2$ species, this is the catalysts containing both Mo and W (i.e. MW25-L and MW50-L).

3.2. Catalytic activity results

3.2.1. Activity

Fig. 7 shows the variation of the catalytic activity with the reaction temperature achieved during the oxidation of a particular chlorinated VOC (trichloroethylene) over catalysts presenting TTB structure and heat-treated at 700 °C (H-series). For comparison, an H-MOR zeolite, that has been described in literature [32] as an active material, has been used as a reference catalyst. In all cases, the trend of catalytic activity is characterized by the light-off curve monitoring the conversion as a function of temperature. Some catalytic tests were repeated with fresh catalysts to check the reproducibility of the experiments.

The catalytic activity of the zeolite reference catalyst (H-MOR) starts at 400 °C and rises up to 80% of TCE conversion at 550 °C. The $T_{50\%}$ (temperature at which 50% conversion was reached) of this catalyst for the oxidative decomposition of trichloroethylene is around 475 °C. In the case of H-series samples, the catalysts which only have Mo or W in their structure show less catalytic activity ($T_{50\%} > 500$ °C) than that achieved over the reference catalyst. On the other hand, the activity of the bronze catalysts containing both Mo and W is higher than that obtained with the zeolite catalyst and present similar conversion values ($T_{50\%}$ of 400 °C and $T_{90\%}$ around 550 °C), in the $0.20 < W/(Mo+W) < 0.80$ composition ratio. These results indicate that the presence of both W and Mo is needed in order to have an active bronze catalyst.

Fig. 8 shows the TCE decomposition light-off curves over the samples heat-treated at 500 °C (L-series). In this case, it can be observed that all the catalysts heat-treated at 500 °C present a lower $T_{50\%}$ and $T_{90\%}$ than those heat-treated at 700 °C. Accordingly, the catalytic activity is higher for the catalysts heat-treated at 500 °C. This behaviour can be related to the higher surface area of the catalysts (Table 1) but also with the results obtained in the TPR characterization (Fig. 4), showing that catalysts heat-treated at 500 °C (L-series) have reduction peaks at ca. 100 °C lower than those achieved for samples heat-treated at 700 °C (H-series).

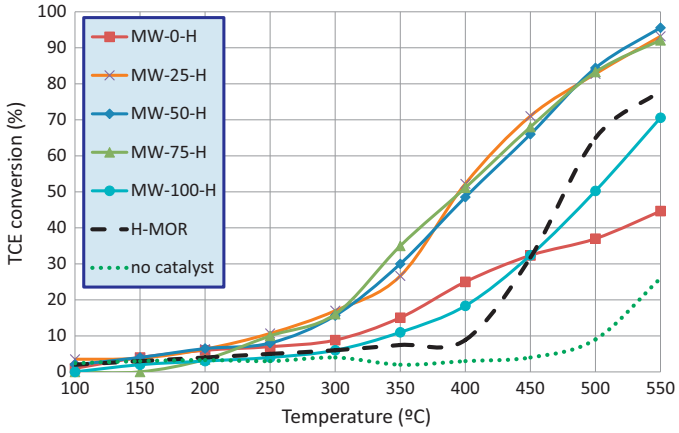

Fig. 7. TCE decomposition light-off curves over bronze catalysts heat-treated at 700 °C (MW-H series).

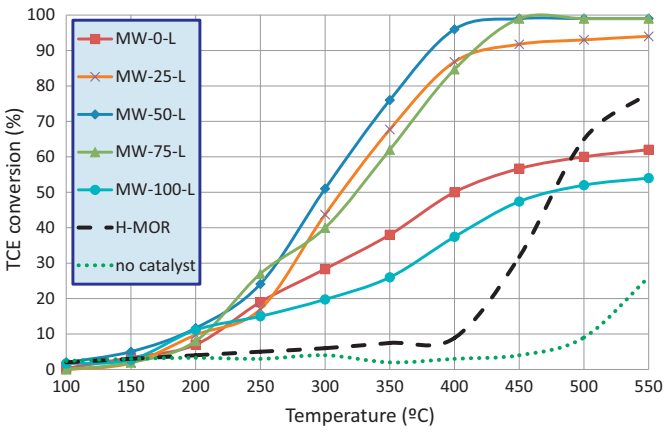

Fig. 8. TCE decomposition light-off curves over bronze catalysts heat-treated at 500 °C (MW-L series).

As observed in Fig. 8, the samples heat-treated at 700 °C containing both Mo and W present a lower $T_{50\%}$ ($T_{50\%}$ around 310 °C) than Mo-free or W-free catalysts ($T_{50\%}$ > 400 °C). These results indicate that together with the surface area and catalyst reducibility, the composition of the catalysts is a key factor in catalytic activity. On the other hand, these catalysts present high values of both $^{16}O^{18}O$ and $^{16}O_2$ in the oxygen-isotopic exchange experiments, which suggests the importance of the diffusion of oxygen species into the bulk. Thus, these catalysts present a higher mobility of oxygen species in their bulk and for this reason, they are the most active ones.

On the other hand, it is also important to discuss the role of the acidity in the activity of the catalysts. According to the NH_3-TPD profiles (Fig. 5A), as the W-content increases, the importance of the second desorption peak in the 250-300 °C range increases, which indicates that when the W-content of the samples increases, the acid strength of the catalyst is higher. Similar results were obtained with the FTIR analysis of adsorbed pyridine that show that Brönsted and Lewis acid sites increased when increasing the W content in the samples.

Some authors suggest the necessity of a combination of both acidity and redox sites for enhancing the catalytic activity in the Cl-VOC oxidation. In this way, Zhou and co-workers [30] studied the activity of Ce_2O/USY catalyst for 1,2-dichloroethane (DCE) oxidation and found that the synergy between acidity and redox sites results in a higher activity. Similar results were found by Gutiérrez-Ortiz et al. [50] who showed that Mn–Zr mixed oxides with surface acidity combined with readily accessible active oxygen species offered higher activity for the oxidation of DCE and TCE. Previously a similar effect was found by same authors [51] for the Ce–Zr mixed oxides. The acidity enhances the adsorption of Cl-VOC on the acid sites of the surface where they are oxidated through the Mars–Van Krevelen mechanism. In this way, if adsorption of chlorinated VOCs is a controlling step, increasing acidity and its strength, will boost the overall rate of the oxidation reaction. On the contrary, very recently Pitkäaho et al. [52,53] suggested that the reducibility of the catalysts and the amount of activated oxygen play a bigger role than acidity in the case of Pt and Pd on Al_2O_3-CeO_2 catalysts for the oxidation of perchloroethylene.

In our case there is not a direct correlation between the acidity of the catalyst and its activity. In fact, the most active catalyst is not the catalyst with highest W-content, but the catalysts containing both W and Mo (MW25, MW50 and MW75). This can be related to the higher mobility of the oxygen species from the bulk to the surface measured by isotopic exchange of $^{18}O_2$. For that reason, although the role of acidity cannot be ruled out, the mobility of oxygen from the bulk to the surface and its total amount is the main parameter that governs activity in the oxidation of TCE in M–W based bronzes.

3.2.2. Selectivity

The main oxidation products obtained with the catalysts in the decomposition of the trichloroethylene were carbon monoxide and hydrogen chloride. Small quantities of intermediate chlorinated by-products, for example chloromethane, dichloromethane, carbon tetrachloride and tetrachloroethylene were found at mild temperatures in the product stream.

Tables 2 and 3 show the product distribution obtained at different temperatures for one of the most active catalyst studied (MW75-L). As it can be seen, CO is the most important product, probably because the temperature is not high enough to oxidize this molecule into CO_2 (Table 2). Nevertheless, as the reaction temperature increases, the formation of CO_2 is favoured although the complete oxidation of the CO is not achieved at 550 °C on these catalysts. Chatterjee and Greene [54] reported similar results with a high selectivity to CO in the oxidation of methylene chloride and trichloroethylene over cobalt exchanged and chromia impregnated Y zeolite catalysts. González-Velasco et al. [55] also reported a high selectivity to CO in the oxidation of 1,2-dichloroethane (DCE) and trichloroethylene (TCE) over H-type zeolites (H-Y and H-ZSM-5), observing also the deposition of carbonaceous material [55–57] on the catalyst surface.

Table 2
Selectivity values towards C-containing products in the combustion of TCE over MW75-L catalyst.

Reaction temperature (°C)	Selectivity[a] (%)		
	CO[b]	CO_2[c]	Other C-products[d]
200	52.9	46.6	0.5
250	54.9	34.1	11.0
300	67.3	19.5	13.2
350	76.2	12.8	11.0
400	89.6	6.9	3.5
450	94.0	5.6	0.4
500	93.1	6.6	0.3
550	89.5	10.3	0.2

[a] Experimental conditions as in Fig. 7.
[b] $S_{CO} = [CO/(CH_3Cl + CH_2Cl_2 + 2C_2Cl_4 + 2C_2H_3Cl + CO_2)] \times 100$.
[c] $S_{CO_2} = [CO_2/(CH_3Cl + CH_2Cl_2 + 2C_2Cl_4 + 2C_2H_3Cl + CO + CO_2)] \times 100$.
[d] $S_{\text{other C-Products}} = 100 - S_{CO} - S_{CO_2}$.

Among all the chlorinated products, HCl is the major reaction product obtained with the MW-75-L catalyst (Table 3) in all the temperature range. At lower temperatures the hydrogen needed to form HCl comes mainly from the TCE feed molecule, however, at higher temperatures the amount of hydrogen present in the feed is not enough to convert all chlorine atoms into HCl. Thus, other sources of hydrogen as water impurities in the feed stream [59] and even hydrogen from the Brönsted sites of the catalyst may be responsible of this effect. When TCE starts to decompose, no Cl_2 is detected at low temperatures, probably because it reacts with TCE to form tetrachloroethylene (C_2Cl_4). At high temperatures (350 °C), this by-product is destroyed and the yield of Cl_2 increases. Bickle et al. [58], Lou and Lee [23] and González-Velasco et al. [55] also obtained similar results in their oxidation reactions.

In addition, it is likely that HCl could be transformed into Cl_2 due to the Deacon reaction. In fact, H-type zeolites are poor Deacon catalysts in comparison with metals which are extremely active for this reaction, leading to the formation of undesired chlorine [60]. We observed that using bronzes catalysts the formation of chlorine is very small, suggesting that these catalysts inhibit the Cl_2 formation through the Deacon process.

In order to study the stability of the samples, some of the catalysts previously studied were tested again at 450 °C in the same conditions. It was observed that the activity and selectivity of these catalysts were the same than before and the catalysts

Table 3
Selectivity values towards Cl-containing products in the combustion of TCE over MW75-L catalyst.

Reaction temperature	Selectivity[a] (%)		
(°C)	HCl[b]	Cl_2[c]	Other Cl-products[d]
200	99.6	0.0	0.4
250	95.6	1.3	3.1
300	79.6	1.3	19.1
350	76.3	1.7	22.0
400	84.9	1.8	13.3
450	96.8	2.5	0.7
500	96.9	2.6	0.5
550	97.0	2.8	0.2

[a] Experimental conditions as in Fig. 7.
[b] $S_{HCl} = [HCl/(CH_3Cl + 2CH_2Cl_2 + 4C_2Cl_4 + C_2H_3Cl + 2Cl_2 + HCl)] \times 100$.
[c] $S_{CO} = [2Cl_2/(CH_3Cl + 2CH_2Cl_2 + 4C_2Cl_4 + C_2H_3Cl + 2Cl_2 + HCl)] \times 100$.
[d] $S_{\text{other C-Products}} = 100 - S_{HCl} - S_{Cl_2}$.

were stable for 6 h of reaction, observing only a small deactivation of the catalysts (from 100% of conversion to 80%) after 10 h of reaction. The characterization by XRD, BET and FTIR of the catalysts after the stability test showed no important changes, indicating that the small deactivation of the catalysts is not related with structural changes but with a small coke deposition on their surface. Nevertheless the coke formation is very low, because if so, the deactivation would be more significant.

4. Conclusions

Mo(W)–Nb–V–P–O mixed oxides with different Mo/W/Nb/V/P atomic ratio have been prepared, heat-treated at different temperatures, characterized and tested in the oxidative decomposition of trichloroethylene.

All of them present a relatively high activity for the removal of TCE in the temperature range studied (350-550 °C). The main reaction products were CO and HCl. Small quantities of intermediate chlorinated by-products were also detected.

The bronzes heat-treated at 500 °C (semi-crystalline mixed oxides) are more active than bronzes heat-treated at 700 °C (presenting tetragonal tungsten bronze (TTB) structure). The different catalytic activity can be explained by the different surface area of the catalysts (which decreases when increasing the heat-treatment temperature) and by the different reducibility (the reduction of catalysts heat-treated at 500 °C is observed at ca. 100 °C lower than those observed for samples heat-treated at 700 °C).

Important differences are also observed in the catalytic behaviour depending on the catalyst composition. Mo,W-containing catalysts present higher catalytic activity than the corresponding samples containing only Mo or W, suggesting that the presence of the pair Mo/W is a key factor in order to have an active catalyst. A good correlation between catalytic activity and $^{18}O_2$ isotopic exchange experiments has been observed. The most active catalysts (samples containing the Mo/W pair) for Cl-VOC oxidation are those presenting relatively high amount of cross labelled $^{16}O^{18}O$ species and high amount of $^{16}O_2$ species, which can be related to a fast diffusion of oxygen species in the surface and into the bulk of the catalysts.

Acknowledgements

The authors wish to thank DGICYT in Spain (Project CTQ2009-14495 and CSD2009-00050-CONSOLIDER/INGENIO 2010) and Universitat Politècnica de València for the financial support. N.B.R. acknowledges Cátedra Cemex Sostenibilidad (UPV) for a fellowship. M.D.S. acknowledges Universitat Politècnica de València for a fellowship.

References

[1] J. Caldwell, R. Lunn, A. Ruder, IARC Monographs on the Evaluation of Carcinogenic Risks to Humans, 1995, pp. 75–158.
[2] J.N. Armor, Applied Catalysis B 1 (1992) 221–256.
[3] I.M. Freidel, A.C. Frost, K.J. Herbert, F.J. Meyer, J.C. Summers, Catalysis Today 17 (1993) 367–382.
[4] Y.S. Matros, G.A. Bunimovich, S.E. Patterson, S.F. Meyer, Catalysis Today 27 (1996) 307–313.
[5] S. Ojala, S. Pitkäaho, T. Laitinen, N. Niskala Koivikko, Topics in Catalysis 54 (2011) 1224–1256.
[6] L. Pinard, J. Mijoin, P. Ayrault, C. Canaff, P. Magnoux, Applied Catalysis B 51 (2004) 1–8.
[7] J.J. Spivey, Industrial & Engineering Chemistry Research 26 (1987) 2165–2180.
[8] S.K. Agarwal, J.J. Spivey, J.B. Butt, Applied Catalysis A 82 (1992) 259–275.
[9] J.B. Butt, J.J. Spivey, S.K. Agrawal, Studies in Surface Science and Catalysis 88 (1994) 19–31.
[10] B. de Rivas, R. López-Fonseca, M.A. Gutiérrez-Ortiz, J.I. Gutiérrez-Ortiz, Applied Catalysis B 104 (2011) 373–381.
[11] B. de Rivas, R. López-Fonseca, M.Á. Gutiérrez-Ortiz, J.I. Gutiérrez-Ortiz, Catalysis Today 176 (2011) 470–473.
[12] B. de Rivas, R. López-Fonseca, C. Jiménez-González, J.I. Gutiérrez-Ortiz, Journal of Catalysis 281 (2011) 88–97.
[13] D. Kießling, R. Schneider, P. Kraak, M. Haftendorn, G. Wendt, Applied Catalysis B 19 (1998) 143–151.
[14] A.M. Padilla, J. Corella, J.M. Toledo, Applied Catalysis B 22 (1999) 107–121.
[15] G. Sinquin, J.P. Hindermann, C. Petit, A. Kiennemann, Catalysis Today 54 (1999) 107–118.
[16] G. Sinquin, C. Petit, S. Libs, J.P. Hindermann, A. Kiennemann, Applied Catalysis B 32 (2001) 37–47.
[17] F. Solymosi, J. Raskó, E. Papp, A. Oszkó, T. Bánsági, Applied Catalysis A 131 (1995) 55–72.
[18] J.J. Spivey, J.B. Butt, Catalysis Today 11 (1992) 465–500.
[19] K. Stephan, M. Hackenberger, D. Kiessling, G. Wendt, Catalysis Today 54 (1999) 23–30.
[20] L. Storaro, R. Ganzerla, M. Lenarda, R. Zanoni, A.J. López, P. Olivera-Pastor, E.R. Castellón, Journal of Molecular Catalysis A: Chemical 115 (1997) 329–338.
[21] J. Corella, J.M. Toledo, A.M. Padilla, Applied Catalysis B 27 (2000) 243–256.
[22] M.M.R. Feijen-Jeurissen, J.J. Jorna, B.E. Nieuwenhuys, G. Sinquin, C. Petit, J.-P. Hindermann, Catalysis Today 54 (1999) 65–79.
[23] J.C. Lou, S.S. Lee, Applied Catalysis B 12 (1997) 111–123.
[24] J.A. Rossin, M.M. Farris, Industrial & Engineering Chemical Research 32 (1993) 1024.
[25] R.W. van den Brink, P. Mulder, R. Louw, Catalysis Today 54 (1999) 101–106.
[26] H. Windawi, Z.C. Zhang, Catalysis Today 30 (1996) 99–105.
[27] S.C. Petrosius, R.S. Drago, V. Young, G.C. Grunewald, Journal of the American Chemical Society 115 (1993) 148–154.
[28] D. Divakar, M. Romero-Sáez, B. Pereda-Ayo, A. Aranzabal, J.A. González-Marcos, J.R. González-Velasco, Catalysis Today 176 (2011) 357–360.
[29] J.I. Gutierrez-Ortiz, R. Lopez-Fonseca, U. Aurrekoetxea, J.R. Gonzalez-Velasco, Journal of Catalysis 218 (2003) 148–154.
[30] Q. Huang, X. Xue, R. Zhou, Journal of Molecular Catalysis A: Chemistry 344 (2011) 74–82.
[31] R. Lopez-Fonseca, A. Aranzabal, J.I. Gutierrez-Ortiz, J.I. Alvarez-Uriarte, J.R. Gonzalez-Velasco, Applied Catalysis B 30 (2001) 303–313.
[32] R. Lopez-Fonseca, J.I. Gutierrez-Ortiz, M.A. Gutierrez-Ortiz, J.R. Gonzalez-Velasco, Journal of Catalysis 209 (2002) 145–150.
[33] P. Botella, J.M. López Nieto, A. Dejoz, M.I. Vázquez, A. Martínez-Arias, Catalysis Today 78 (2003) 507–512.
[34] P. Botella, E. García-Gonzalez, A. Dejoz, J.M. López Nieto, M.I. Vázquez, J. González-Calbet, Journal of Catalysis 225 (2004) 428–438.
[35] M.D. Soriano, P. Concepción, P. Botella, J.M. López Nieto, Topics in Catalysis 54 (2011) 729.
[36] R.D. Shanon, Acta Crystallographica Section A 32 (1976) 751.
[37] P. Botella, B. Solsona, J.M. López Nieto, P. Concepción, J.L. Jordá, M.T. Doménech-Carbó, Catalysis Today 158 (2010) 162–169.
[38] P. Botella, E. García-González, B. Solsona, E. Rodríguez-Castellón, J.M. González-Calbet, J.M. López Nieto, Journal of Catalysis 265 (2009) 43–53.
[39] J. Holmberg, J.B. Wagner, R. Häggblad, S. Hansen, L.R. Wallenberg, A. Andersson, Catalysis Today 128 (2007) 153–160.
[40] V.R. Porter, W.B. White, R. Roy, Journal of Solid State Chemistry 4 (1972) 250–254.
[41] J.M. Oliver, J.M. López Nieto, P. Botella, A. Mifsud, Applied Catalysis A 257 (2004) 67–76.
[42] H. Aritani, T. Tanaka, T. Funabiki, S. Yoshida, K. Eda, N. Sotani, M. Kudo, S. Hasegawa, The Journal of Physical Chemistry 100 (1996) 19495.
[43] J.M.R. Gallo, I.S. Paulino, U. Schuchardt, Applied Catalysis A 266 (2004) 223–227.
[44] A. de Lucas, J.L. Valverde, P. Cañizares, L. Rodriguez, Applied Catalysis A 172 (1998) 165–176.
[45] D.G. Barton, M. Shtein, R.D. Wylson, S.L. Soled, E. Iglesia, The Journal of Physical Chemistry B 103 (1999) 630–640.
[46] T. Debnath, S. Roy, C.H. Rüscher, A. Hussain, Journal of Materials Science 44 (2009) 179–185.
[47] G.R. Bamwenda, H. Arakawa, Applied Catalysis A 210 (2001) 181–191.
[48] C.v.S. Liesel Harmse, E. van Steen, Catalysis Letters 137 (2010) 123–131.
[49] P. Concepción, S. Hernández, J.M.L. Nieto, Applied Catalysis A 391 (2011) 92–101.
[50] J.I. Gutierrez-Ortiz, R.B. de, R. Lopez-Fonseca, S. Martin, J.R. Gonzalez-Velasco, Chemosphere 68 (2007) 1004–1012.
[51] R. López-Fonseca, J.I. Gutiérrez-Ortiz, M.A. Gutiérrez-Ortiz, J.R. González-Velasco, Catalysis Today 107–108 (2005) 200–207.
[52] S. Pitkäaho, L. Matejova, K. Jiratova, S. Ojala, R.L. Keiski, Applied Catalysis B 126 (2012) 215–224.
[53] S. Pitkäaho, L. Matejova, S. Ojala, J. Gaalova, R.L. Keiski, Applied Catalysis B 113–114 (2012) 150–159.
[54] S. Chatterjee, H.L. Greene, Applied Catalysis A 98 (1993) 139–158.
[55] J.R. González-Velasco, A. Aranzabal, R. López-Fonseca, R. Ferret, J.A. González-Marcos, Applied Catalysis B 24 (2000) 33–43.
[56] S. Chatterjee, H.L. Greene, Y.J. Park, Catalysis Today 11 (1992) 569–596.
[57] S. Imamura, H. Tarumoto, S. Ishida, Industrial & Engineering Chemical Research 28 (1989) 1449.
[58] G.M. Bickle, T. Suzuki, Y. Mitarai, Applied Catalysis B 4 (1994) 141–153.
[59] J.R. González-Velasco, R. López-Fonseca, A. Aranzabal, J.I. Gutiérrez-Ortiz, P. Steltenpohl, Applied Catalysis B 24 (2000) 233–242.
[60] J.R. Gonzalez-Velasco, A. Aranzabal, J.I. Gutierrez-Ortiz, R. Lopez-Fonseca, M.A. Gutierrez-Ortiz, Applied Catalysis B 19 (1998) 189–197.